ADVANCED FUNCTIONAL MATERIALS
www.afm-journal.de

On-Surface Indigo-Based Bimolecular Coordination Networks with Programmable Regular or Vitreous Structure

Hongxiang Xu, Ritam Chakraborty, Biao Yang, Dennis Meier, Joachim Reichert, Svetlana Klyatskaya, Mario Ruben, Shobhana Narasimhan,* Johannes V. Barth,* and Anthoula C. Papageorgiou**

Fabrication of diverse and complex 2D molecular architectures using surface-confined supramolecular coordination chemistry has been continuously attracting considerable attention for years. Here, the on-surface synthesis of 2D coordination networks exhibiting both crystalline and vitreous phases employing the same constituents is reported. Robust and flexible bimolecular 2D coordination networks, structurally analogous to 2D bilayer silica films on Ru(0001) and graphene, are achieved by iron-directed self-assembly of indigo and 1,3,5-tris[4-(pyridin-4-yl)phenyl]benzene (ext-TPyB) or 1,3,5-tris(pyridyl)benzene (TPyB) linkers on Au(111). The crystalline phase features honeycombed nanopores, displaying long-range order with local defects that can be attributed to variations in coordination nodes and shape flexibility of the ext-TPyB (/ TPyB) ligand. The vitreous phase evolves upon annealing the honeycomb network to higher temperatures and exhibits reticulated polygons similar to Zachariasen's 2D random network theory. The size of the polygons follows a lognormal distribution, with the probability density function showing an almost linear behavior as characteristic of the structure of glass. The results enrich avenues toward the fabrication and understanding of novel nanostructured condensed matter systems, such as 2D crystalline and vitreous structures, as well as provide the unique possibility to understand structurally bulk glasses.

1. Introduction

Elucidating the structure of complex condensed matter phases such as glasses, glassy crystals, quasicrystals, and protein and virus crystals is a key factor in understanding their properties and behavior, and for developing novel materials.[1–6] Among such materials, the atomic structure of silica glass has been a fascinating issue since William H. Zachariasen published in 1932 his postulates (2D random network theory) on "The Atomic Arrangement in Glass".[7] His hypothesis was universally accepted and became the standard textbook model. The invention of scanning tunnelling microscopy (STM) provided access to high local resolution to identify single adsorbates (atoms and molecules) and 2D structures on the surface in real space.[8–9] Recently, 2D glasses of bilayers of vitreous and crystalline silica have been synthesized successfully on the Ru(0001) surface and observed in situ using STM.[10–12] The bilayer of vitreous silica

H. Xu, B. Yang, D. Meier, J. Reichert, J. V. Barth, A. C. Papageorgiou
Physics Department E20
School of Natural Sciences
Technical University of Munich
James Franck Strasse 1, 85748 Garching, Germany
E-mail: joachim.reichert@tum.de; jvb@tum.de; a.c.papageorgiou@chem.uoa.gr

H. Xu
School of Electronics
Peking University
Beijing 100871, China

R. Chakraborty, S. Narasimhan
Theoretical Sciences Unit
Jawaharlal Nehru Centre for Advanced Scientific Research
Jakkur, Bangalore 560054, India
E-mail: shobhana@jncasr.ac.in

B. Yang
State Key Laboratory of Bioinspired Interfacial Materials Science
Institute of Functional Nano and Soft Materials (FUNSOM)
Soochow University
Suzhou 215123, China

D. Meier
Department of Chemistry
Tufts University
Medford, MA 02155, USA

The ORCID identification number(s) for the author(s) of this article can be found under https://doi.org/10.1002/adfm.202512253

DOI: 10.1002/adfm.202512253

exhibited a complex ring network with a lognormal ring size distribution[13–14] in good agreement with Zachariasen's 2D random network theory.[11]

Surface-confined supramolecular coordination chemistry[15–18] has provided new ways to engineer a diversity and complexity of molecular architectures by exploiting the metal-directed assembly of molecular linkers on planar surfaces. Notable examples of our endeavors include the self-assembly of nonlinear, prochiral, ditopic dicarbonitrile linkers and Co atoms in random 2D string networks with diverse coordination nodes on Ag(111).[19–20] By exploiting related ditopic linkers and the increased coordination sphere offered by lanthanides, five-vertex Archimedean surface tessellations form on Ag(111) with Ce,[21] and quasicrystalline tilings form on Au(111) with Eu.[22] Bicomponent supramolecular systems on surfaces offer further flexibility in triggering and controlling the assembly.[23–25] Hitherto, there are only a handful of reports of coordination networks featuring two different molecular ligands, often termed as "multicomponent supramolecular coordination networks". The first used ditopic carboxylate linkers, ditopic pyridine ligands, and Fe.[26] The second features the combination of a ditopic terpyridine ligand and a tetratopic pyridine ligand: with Fe on Au(111), two network polymorphs (a rhombus and a Kagome) self-assemble.[27] And another example is Eu linked ditopic nitriles and ditopic terpyridines on Au(111).[28] More recently, two different tritopic pyridine linkers were combined with native Cu adatoms on Cu(111), giving rise to a range of reticular disordered networks depending on the linker stoichiometry.[29] Moreover, pyridine linkers have been employed in supramolecular short-range disordered crystalline networks on Ag(111).[30] From these, we notice that pyridine ligands seem to enable multicomponent networks and structural adaptability in the self-assembly.

S. Klyatskaya, M. Ruben
Institute of Nanotechnology
Karlsruhe Institute of Technology (KIT)
Hermann-von-Helmholtz-Platz 1, 76344 Eggenstein-Leopoldshafen, Germany

M. Ruben
Institute of Quantum Materials and Technologies (IQMT)
Karlsruhe Institute of Technology (KIT)
Hermann-von-Helmholtz-Platz 1, 76344 Eggenstein-Leopoldshafen, Germany

M. Ruben
Centre Européen de Sciences Quantiques (CESQ)
Institut de Science et d'Ingénierie Supramoléculaires (ISIS)
8 allée Gaspard Monge, BP 70028, Strasbourg, Cedex 67083, France

S. Narasimhan
School of Advanced Materials
Jawaharlal Nehru Centre for Advanced Scientific Research
Jakkur, Bangalore 560054, India

S. Narasimhan
International Centre for Theoretical Sciences
Shivakote, Hesaraghatta Hobli, Bengaluru 560080, India

A. C. Papageorgiou
Laboratory of Physical Chemistry
Department of Chemistry
National and Kapodistrian University of Athens
Panepistimiopolis, Athens 15771, Greece

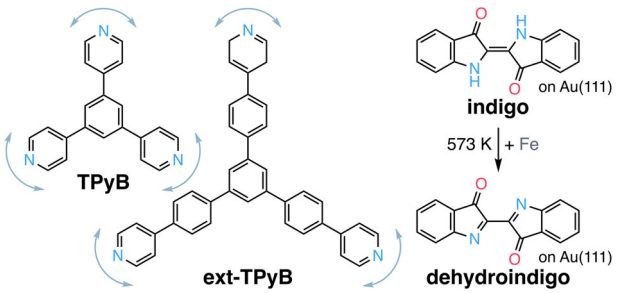

Figure 1. Ligands of the present investigation: TPyB, ext-TPyB, and dehydroindigo obtained from indigo. Curved arrows indicate the flexibility of the pyridyls.

We recently reported that indigo molecules can be ditopic chelating linkers in Fe coordination polymers on Ag(111).[31] Indigo (**Figure 1**) is a traditional dye that is being repurposed due to its molecular properties.[32–38] Applications include redox-[39] and electro-[40] chemistry, redox-switchable ionophores[41–42] and batteries.[40] Advantages such as biocompatibility and biodegradability offered by natural compounds have attracted their use in coordination networks. Hitherto, there are examples of 2D coordination networks of functionalized porphyrins,[43–44] DNA bases[45] and peptides.[46] Inspired by the advances in 2D coordination networks outlined above, here we combined indigo and tritopic pyridine linkers with Fe on a planar metal surface, in order to expand from the 1D coordination polymer to the porous 2D coordination network.

In particular, we investigate the self-assembly of Fe coordination networks on Au(111) using indigo and 1,3,5-tris[4-(pyridin-4-yl)phenyl]benzene (ext-TPyB) or 1,3,5-tris(pyridyl)benzene (TPyB) linkers (Figure 1). A STM study, supported by X-ray photoelectron spectroscopy (XPS) measurements and density functional theory (DFT) investigations, sheds light on the intricate self-assembly scenario that emerges. We report on fabricating thermally robust bimolecular 2D coordination networks with tunable pore size featuring crystalline and vitreous phases, bearing similarities with the aforementioned 2D bilayer silica films on both Ru(0001)[10] and graphene.[47] Importantly, our findings provide a model system for the topical materials of metal-organic framework glasses,[48] where the structural characteristics can be conveniently interrogated and manipulated at the single molecule level with STM.

2. Results and Discussion

2.1. Crystalline Phase of Dehydroindigo$_3$(ext-)TPyB$_2$Fe$_6$

When indigo, (ext-)TPyB, and Fe are deposited sequentially on the Au(111) surface and are subjected to annealing at 623 K, crystalline 2D honeycomb phases can be synthesized (**Figure 2**, large-scale STM in Figure S1 (Supporting Information), room temperature (r.t.), imaging in Figure S2 (Supporting Information)). Figure S1 (Supporting Information) shows images representative of the overall surface, which contain a global molecular ratio of indigo to (ext-)TPyB of ≈1.5, displaying ordered 2D honeycomb islands more than 200 nm across, free Au areas, and very limited regions of irregularly arranged molecules.

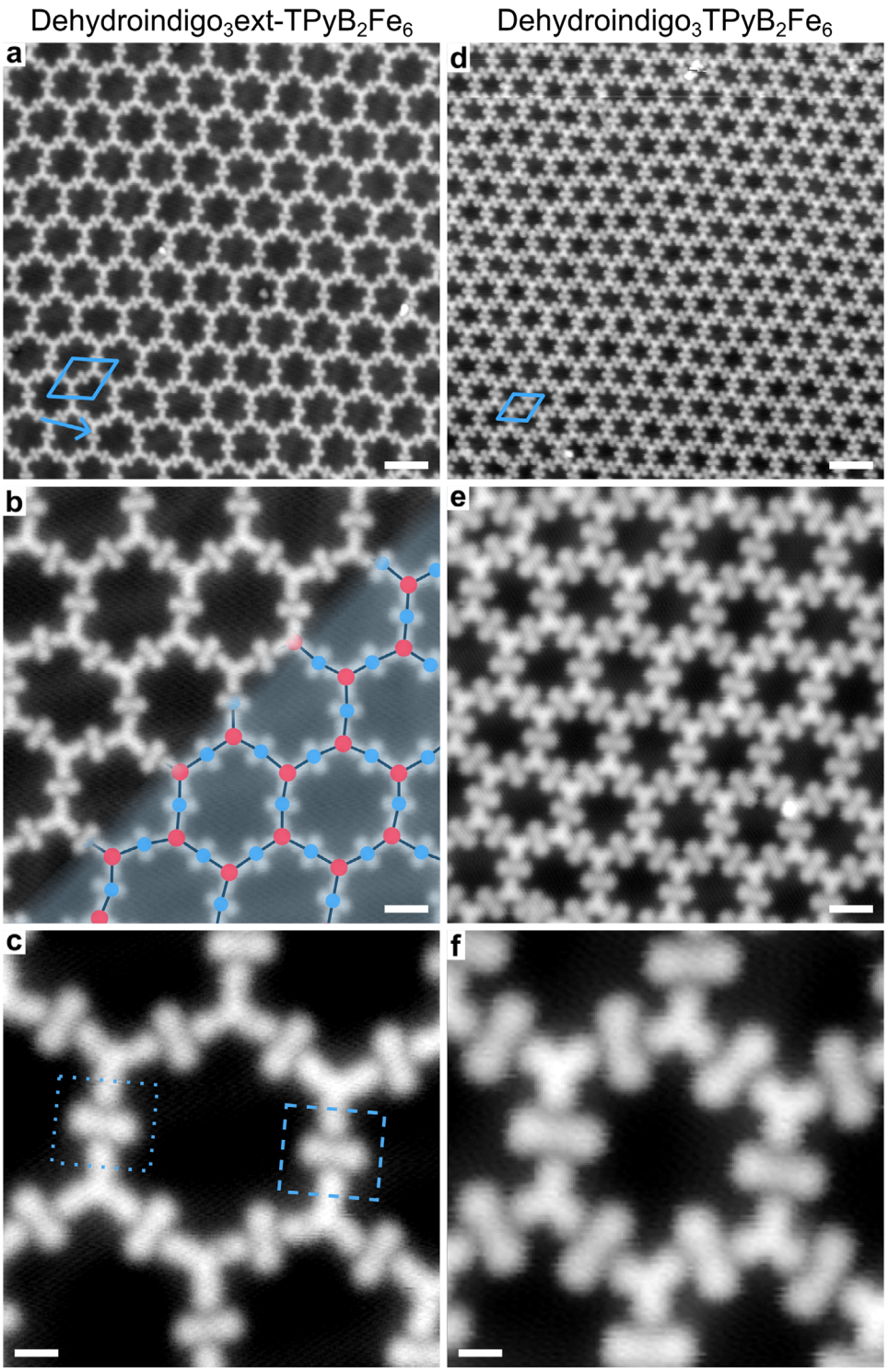

Figure 2. STM images showing the formation of the crystalline phases (2D honeycomb nanopore networks) after annealing indigo, (ext-)TPyB, and Fe on Au(111) to 623 K in different magnifications. a–c) Dehydroindigo$_3$ext-TPyB$_2$Fe$_6$. In the bottom right corner of (b), the building block connectivity and the network are depicted, with blue markings at the centres of dehydroindigo and red dots at the centres of ext-TPyB. d–f) Dehydroindigo$_3$TPyB$_2$Fe$_6$. The rhombi in (a) and (d) mark the unit cells. The arrow in (a) indicates the Au [1$\bar{1}$0] direction. The white scale bars are 5 nm in (a,d), 2 nm in (b,e), 1 nm in (c), and 0.7 nm in (f). Imaging parameters: (a) −100 mV, 100 pA; (b-c) 5 mV, 100 pA; (d–e) −800 mV, 300 pA; (f) 10 mV, 100 pA.

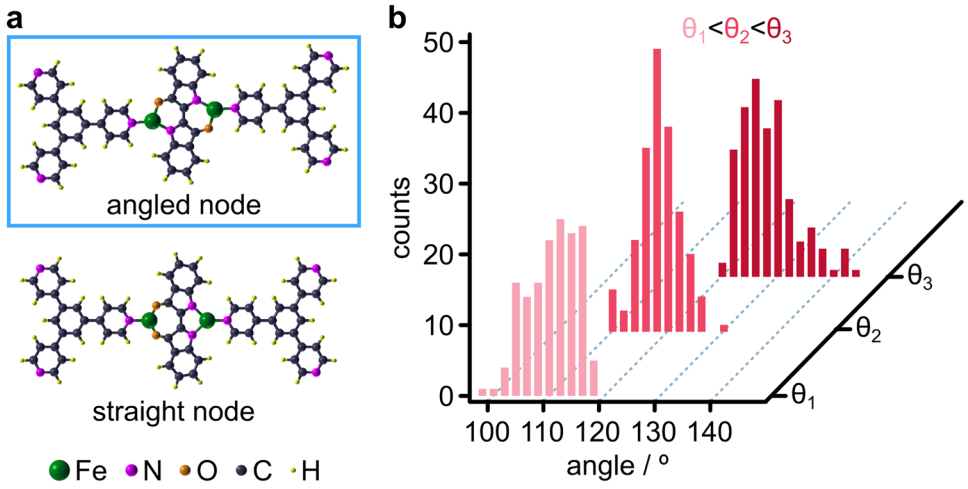

Figure 3. Variations of the coordination nodes and flexibility of the crystalline network. a) Optimized structural models of Fe-coordination nodes. Top: the more stable angled node with *trans*-dehydroindigo. Bottom: the less stable straight node with *cis*-dehydroindigo. b) Distributions of the three opening angles of ext-TPyB in the crystalline indicated by θ_1, θ_2, and θ_3, respectively.

The periodicity of the hexagonal network is 3.58 nm for TPyB and increases by ≈43% to 5.13 nm when replacing TPyB with ext-TPyB. The honeycomb pores exhibit a characteristic registry on the Au(111) with their unit cell rotated by 15° with respect to the Au(111) high-symmetry axis. The chevron reconstruction of Au(111) is detectable under the network. All symmetrically equivalent domains (including the mirror symmetry with 45° rotation with respect to the Au [1$\bar{1}$0] direction, Figure S3 (Supporting Information), were found in our STM investigation. High-resolution STM images in Figure 2c,f provide a direct identification of the molecular building blocks of a single honeycomb motif. The dumbbell shaped features are consistent with the size and expected shape of the indigo monomers, while the (ext-)TPyB are hallmarked by their triangular shapes.

XPS measurements provided insights into the chemical structure of the assembled molecules. The N 1s spectrum (Figure S4, Supporting Information) exhibits a single peak at 399.3 eV after mixing indigo and ext-TPyB on the surface at r.t. due to the overlapping contributions of the indigo -NH group[49] and the pyridine N atom.[50–51] With the addition of a small amount of Fe to the surface, Fe coordination with iminic N appears, signified by an additional signal located at 398.2 eV in Figure S4 (Supporting Information). This additional signal reflects a small portion of the total N atoms of the system, indicating that annealing is needed to promote the N—H bond cleavage in indigo and have the dehydroindigo form which engages in surface coordination nodes.[31] Indeed, following sample annealing at 573 K, all N atoms are iminic and coordinated to Fe adatoms (single peak at 398.1 eV, Figure S4, Supporting Information).[49] The O 1s spectrum also confirms the Fe coordination by the shift of the indigo carbonyl group (C═O) to higher binding energy (Figure S5, Supporting Information).[52] Hence, we deduce that these networks are composed of dehydroindigo (indigo following N—H bond scissions, Figure 1) and (ext-)TPyB coordinated by Fe atoms.

Given the Fe coordination indicated by the XPS data and the geometry of the molecular building blocks, we propose single Fe atoms in each coordination node between dehydroindigo and (ext-)TPyB. The experimentally observed honeycomb structure has long-range order with frequent irregularities. This local disorder is attributed to variations of the coordination nodes[53] and shape flexibility[30] of (ext-)TPyB. Molecules forming local stoichiometric defects, i.e., molecules trapped within the pores or involved in homoleptic coordination motifs, represent only ≈0.5% of the total molecules in the crystalline domains. We modelled the nodes by a *trans*-dehydroindigo placed between two Fe-TPyB units (DFT optimized geometries in **Figure 3a**, top and Figure S6a, Supporting Information) and by a *cis*-dehydroindigo between two Fe-TPyB units (DFT optimized geometries in Figure 3a, bottom and Figure S6f, Supporting Information), both in the gas phase and on the Au(111) surface. The former is found to be energetically favored by 224 meV in the gas phase and by 400 meV when placed on Au(111). A Bader charge analysis reveals that in these nodes each Fe atom donates 1.20 e^- (mainly to the coordinating N atom of dehydroindigo). The charge accumulation on Fe is largely maintained (1.19 e^-) upon adsorption on Au(111), which is in line with the oxidation shift of the Fe $2p_{3/2}$ peak observed in the XPS data (Figure S4, Supporting Information).[54–56]

The majority of the observed nodes have the geometry of the energetically favored "angled node" (indicated by dotted and dashed rectangles in Figure 2c), consistent with the simulated STM images obtained from DFT data for nodes placed on the Au(111) substrate (Figure S6, Supporting Information). This node has two surface enantiomers, which seem to be randomly expressed without any periodicity. A minority of the nodes (≈12%) can be identified as "straight nodes" (red rectangles in Figure S7, Supporting Information). A plausible explanation for the appearance of the *cis*-dehydroindigo node might be the interaction with the Au(111) substrate. Indeed, DFT optimizations of the molecular structure with the *trans*-dehydroindigo (Figure 3a, top) on Au(111) at different adsorption sites found variations of 538 meV in energy. We further observe that the triangular linker shows significant structural flexibility: the opening angles between pyridin-4-phenyl groups range from

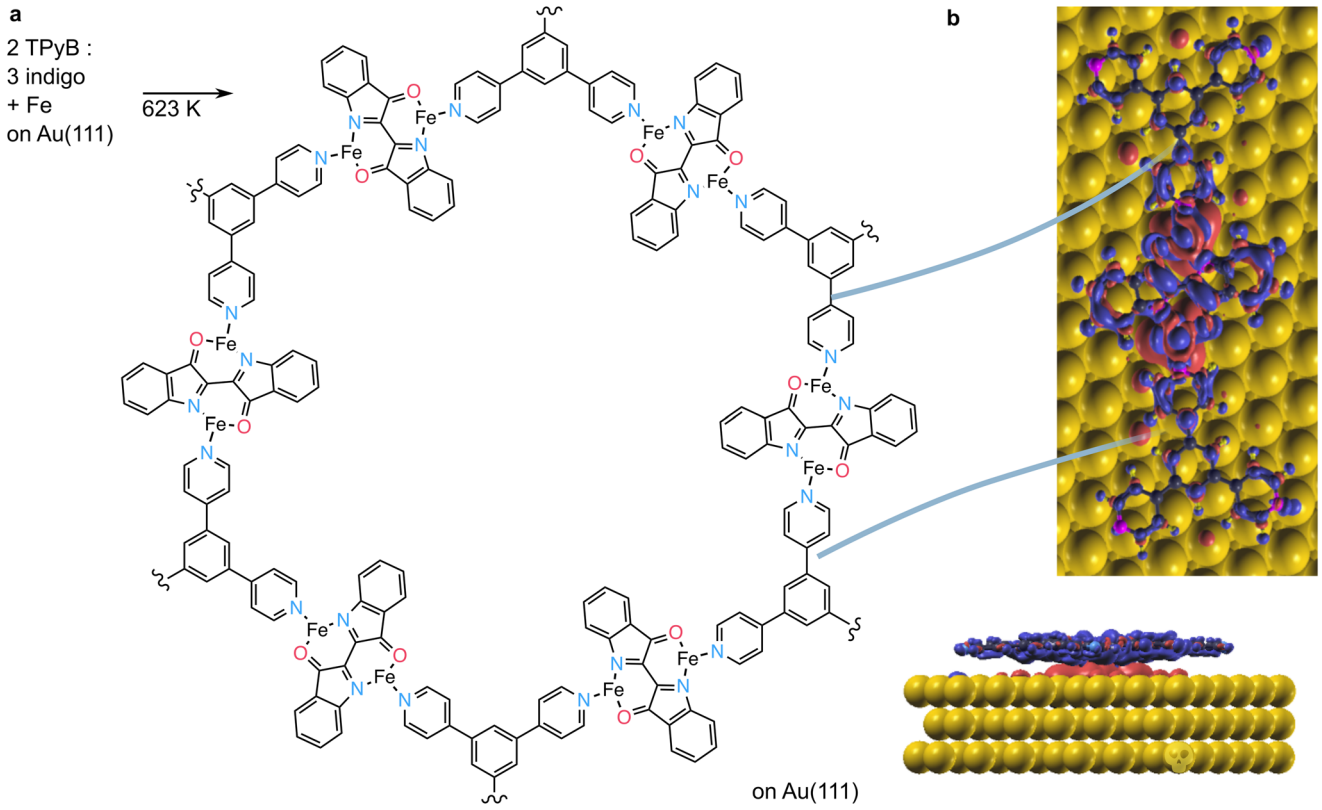

Figure 4. a) Synthesis scheme of 2D honeycomb coordination network on Au(111). b) Top view and side view of the charge density difference plot of the adsorbed network motif on Au(111). The constant differential charge density contours are plotted at a value of 9×10^{-4} e bohr^{-3}. Red and blue lobes signify e$^-$ accumulation and depletion, respectively. The Au substrate atoms are denoted by yellow spheres.

98° to 145° (Figure 3b). This allows for the expression of local disorder, whereas long range order is maintained. This flexibility is further demonstrated by tip manipulation experiments of both ext-TPyB in isolated coordination complexes (Figure S8, Supporting Information) and of dehydroindigo in the honeycomb network (Figure S9, Supporting Information). Notably, within the 2D coordination network, it is possible to manipulate and vary individual nodes with the STM tip, while maintaining the connectivity of the network components.

The previously unreported coordination motif constituting the crystalline phase (**Figure** 4a) and its interaction with the Au(111) substrate were also investigated by computational modelling. Notably, for the energy optimized node with *trans*-dehydroindigo placed on unreconstructed Au(111), a Bader charge analysis reveals a 1.48 e$^-$ donation from the coordination motif to the substrate, indicating substantial interactions (Figure 4b).

2.2. Vitreous Phase of Dehydroindigo$_3$(ext-)TPyB$_2$Fe$_6$

The influences of the relative concentration between the two molecular building blocks, i.e., indigo and (ext-)TPyB, and the annealing temperature on the reaction products were investigated systematically. We performed experiments where different compositions of indigo, TPyB, and Fe were gradually annealed on Au(111). Figure S10 (Supporting Information) shows a case where the coverage of TPyB is more than that of indigo, with an initial ratio of ≈3 indigo: 4 TPyB. Following annealing at 423 K, we found the coexistence of (i) a network featuring the same local bonding schemes as in the honeycomb network but exhibiting no long-range order and (ii) segregation of TPyB islands bonded by three-fold Fe-coordination.[57] After annealing at 523 K, we obtained extended domains of the honeycomb network coexisting with the TPyB islands and a surface ratio of ≈1 indigo: 1 TPyB. Further annealing at 623 K resulted in a surface ratio of 3 indigo: 2 TPyB and the exclusive formation of the honeycomb network. The TPyB islands dissolve, presumably due to desorption of the TPyB not retained in the adsorbed honeycomb network. This finding is particularly noteworthy, as it indicates that the adsorbed honeycomb network has a thermal stability of more than 623 K, which is further supported by the tip manipulation experiments (Figure S9, Supporting Information). Similar results are found upon the gradual addition of TPyB to the Fe coordinated indigo chains on Au(111) (Figure S11, Supporting Information). Overall, homoleptic coordination nodes form when there is an excess of one type of ligand, and heteroleptic coordination nodes are preferred given the availability of both types of ligands, indicating a thermodynamically favored assembly. In the corresponding experiments with ext-TPyB, some small portion of the disordered network was also observed following annealing at 623 K (Figure S12, Supporting Information).

Of particular interest are the disordered network elements obtained after annealing at 423 K (Figure S10a, Supporting Information). Surprisingly, the crystalline honeycomb structure of

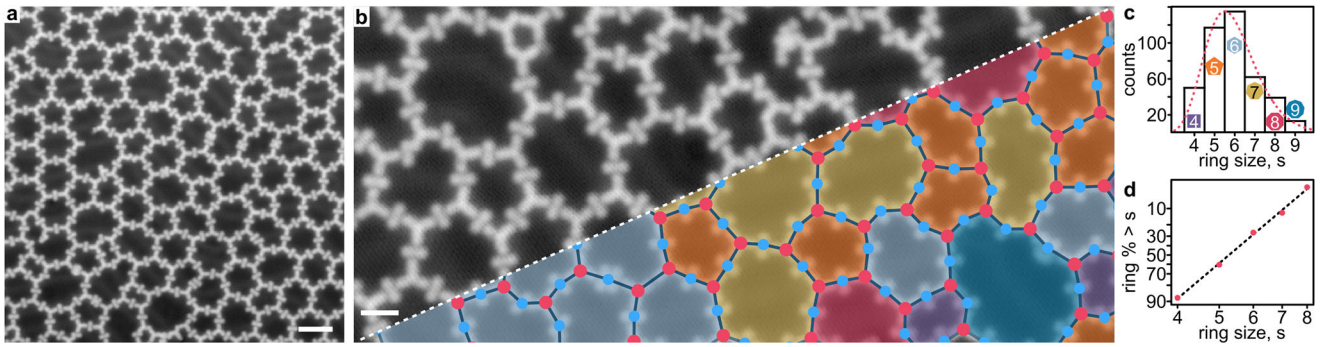

Figure 5. Formation of the vitreous phase (2D random network) after annealing dehydroindigo$_3$ext-TPyB$_2$Fe$_6$ on Au(111) at 673 K. a) Overview STM image with the network of polygons. b) Magnified STM image. In the bottom right corner, the building block connectivity and the network are depicted in analogy to the silica glass, with blue marking the centre of dehydroindigo and red the centre of ext-TPyB. c) The ring size distribution of the amorphous network (425 rings in total). The red dashed line represents a lognormal fit to the data. d) A lognormal plot of the probability density function of the ring size distribution in (c).[60] Imaging parameters: (a, b) 100 mV, 100 pA. The white scale bars are 5 nm in (a) and 2.5 nm in (b).

dehydroindigo$_3$(ext-TPyB)$_2$Fe$_6$ also converts to an overall disordered network after annealing at 673 K (**Figure** 5a,b; Figures S13 and S14, Supporting Information). The high-temperature annealing is presumably required in order to melt the formed network, in line with the vitrification process. This vitreous phase is thermally stable at r.t. (Figures S10a and S15, Supporting Information) and its formation reflects a reduced surface density of molecular constituents, expanding into the free Au areas (observed in Figure S1, Supporting Information). A close inspection reveals predominantly the same coordination bonding features as in the ordered phase, accompanied by a loss of long-range order. The molecular ratio of dehydroindigo to ext-TPyB is measured in overview STM images recorded at 5 K as 1.49 ± 0.11, matching the stoichiometry of the crystalline phase. The formation of a vitreous phase is the fingerprint of competing structures with the same composition and similar formation energies.[58] The reciprocal space of the crystallographic data of silica can be compared with the fast Fourier transformations of the STM data (Figure S16, Supporting Information). The crystalline long-range order of the honeycomb network is evident by sharp spots. For the glassy phase, these spots are absent. We notice that for the silica glass, reciprocal space data are characterized by a ring reflecting the Si—O bonding distances.[59] In our case, the appearance of the diffused ring represents the transition of the honeycomb lattice to a glassy phase. Noticing the similarity of this phase with Zachariasen's scheme of a random network,[7] a similar analysis is applied.

Figure 5b (more extended in Figure S14, Supporting Information) visualizes the different polygons, which range mostly from a tetragon to a nonagon. A statistical analysis of the ring size, given by the number of polygon sides, is presented in Figure 5c. The distribution is very similar to that observed in the vitreous phase of a bilayer SiO_2 film on Ru(0001)[10,12,61] or graphene.[47] The pentagon rings are more abundant than the heptagon rings, while the tetragons occur more frequently than the octagon rings. It is a general tendency observed throughout many different STM images that the ring size distribution does not follow a Gaussian distribution, but is asymmetric with respect to the most abundant species (the hexagon ring). This distribution can be described by a lognormal distribution function, which exhibits a linear behavior in a lognormal probability plot (Figure 5d) that is regarded as an inherent feature of the connectivity requirements of the 2D random network structure.[13] Last but not least, we also observe crystalline-vitreous interfaces (Figure S17, Supporting Information). It can be seen that the first rings to appear close to the crystalline area of hexagons are pentagons and heptagons, which is in good agreement with the reported analysis of crystalline-vitreous interfaces in 2D silica.[62]

3. Conclusion

In summary, we have demonstrated the fabrication of thermally robust and flexible bimolecular 2D coordination networks of tunable pore size bearing crystalline and vitreous-like phases on a noble metal surface. This is achieved by using a bimolecular coordination assembly of indigo and (ext-)TPyB linkers stabilized by a previously unreported coordination motif which comprises single Fe atoms by a chelating dehydroindigo and a pyridine. Within this coordination, individual nodes are addressable by the STM tip and can be manipulated without decomposition. The crystalline phase is a 2D honeycomb network, exhibiting short-range disorder that can be attributed to the variability of the coordination node configuration. Under different preparation conditions, a vitreous phase, described by Zachariasen's scheme of a random network, can form. The distribution of ring sizes follows a lognormal distribution, which is regarded as an inherent consequence of the connectivity requirements of the 2D random network.[61] Our results provide new avenues toward the fabrication and understanding of novel nanostructured condensed matter systems, such as 2D crystalline and vitreous structures. Moreover, the possibility to interrogate such model systems at the single molecule level by scanning probe microscopy methods offers unique possibilities to understand the structures and properties of bulk glasses.

4. Experimental Section

Synthesis: The compounds TPyB and ext-TPyB, depicted in Figure 1, were synthesized via a palladium-catalyzed Suzuki coupling. Detailed information about the synthesis can be found in the Supporting Information.

Sample Preparation: Samples were prepared in situ in three different ultra-high vacuum preparation chambers attached to the analysis

chambers hosting either a Joule Thomson STM, a variable temperature STM or an XPS system, described below. In all preparations the clean Au(111) single crystal surface was subjected to multiple cycles of Ar^+ sputtering and annealing at 700 K. Indigo (TCI, exceeding 97% dye content), TPyB and ext-TPyB were deposited on the r.t. Au(111) surface by organic molecular beam epitaxy (OMBE) by heating the solid powders at ≈493–523 K, 483 K and 553 K, respectively.

Scanning Tunnelling Microscopy: STM measurements were carried out with chemically etched W tips with tunnelling bias referring to the sample bias. Measurements were performed at ≈4.6 K by a Joule-Thomson STM or at r.t. by a variable temperature Aarhus-type STM (both by SPECS GmbH). Data presented here were recorded at 4.6 K, unless mentioned otherwise. WSxM[63] and SpmImage Tycoon[64] were used for the data analysis and representation.

X-Ray Photoelectron Spectroscopy: The measurements were performed in a SPECS GmbH UHV system at the Technical University of Munich – Walter Schottky Institute laboratory. The X-ray source was monochromatic Al Kα ($h\nu = 1486.71$ eV). Photoemitted electrons were collected by a SPECS Phoibos 150 hemispherical analyser in normal emission geometry. The energy scale was calibrated by setting the Au $4f_{7/2}$ peak at a binding energy of 84.0 eV.

Density Functional Theory calculations: All the calculations were performed using spin-polarized DFT as implemented in the Quantum Espresso software package.[65] Interactions between the ionic cores and the valence electrons have been described using the Projector Augmented Wave (PAW) method.[66] The vdw-DF2-B86R functional[67–68] was used to incorporate the gradient corrected exchange potential and the non-local van der Waals interactions in the system. The strong correlations of the partially filled Fe-3d orbitals were treated using the LSDA+U[69] approach with a Hubbard onsite parameter, $U = 4$ eV. The Kohn-Sham wavefunctions and charge densities were expanded in a plane-wave basis set with a kinetic energy cutoff of 60 Ry and charge density cutoff of 300 Ry.

The Au(111) surface was modelled using an asymmetric slab three atomic layers thick. In the case of the node with *trans*-dehydroindigo ("angled" node) on the Au(111) surface, a surface supercell characterized by the supercell matrix $\begin{pmatrix} 8 & 2 \\ 4 & 14 \end{pmatrix}$ was used. For modelling the coordination node with *cis*-dehydroindigo ("straight" node) on Au(111), a surface was considered supercell characterized by a supercell matrix $\begin{pmatrix} 7 & 0 \\ 7 & 14 \end{pmatrix}$. The upper two layers of Au(111) and all overlayer coordinates were allowed to relax using Broyden-Fletcher-Goldfarb-Shanno (BFGS)[70–73] algorithm until all force components on all atoms were less than 0.001 Ry/Bohr, while the lowest layer of the Au(111) slab was kept fixed. Brillouin zone sampling was restricted only to the gamma point for all geometry optimization calculations employing the Au(111) surface and Marzari-Vanderbilt cold smearing[74] of width 0.005 Ry was applied in all calculations. The STM simulations were performed using the Tersoff-Hamann approach.[75]

Supporting Information

Supporting Information is available from the Wiley Online Library or from the author.

Acknowledgements

The authors acknowledge funding of the German Research Foundation (DFG) through the priority program COORNETs (SPP1928) with project number 316890188 and the framework of H.F.R.I. Call "Basic Research Financing (Horizontal support of all Sciences)" under the National Recovery and Resilience Plan "Greece 2.0" funded by the European Union—NextGenerationEU (H.F.R.I. Project Number: 15609). Support and resources were provided by the PARAM Yukti, National Supercomputing Mission and TUE-CMS, both at JNCASR, Bangalore, India. H.X. thanks the China Scholarship Council (CSC) for a doctoral scholarship. B.Y. acknowledges the Collaborative Innovation Center of Suzhou Nano Science & Technology, the Suzhou Key Laboratory of Surface and Interface Intelligent Matter (Grant SZS2022011), and the 111 Project. M.R. and S.K. acknowledge Karlsruhe Nano Micro Facility (KNMFi,), a Helmholtz Research Infrastructure at Karlsruhe Institute of Technology (KIT), Germany and financial support from the CNRS research infrastructure INFRANALYTICS (FR2054) for conducting the research. S.N. also acknowledges the Sheikh Saqr Laboratory of ICMS, JNCASR, and the Anna Boyksen Fellowship of the Technical University of Munich, Institute for Advanced Study. The publication of the article in OA mode was financially supported by HEAL-Link.

Conflict of Interest

The authors declare no conflict of interest.

Data Availability Statement

The data that support the findings of this study are available from the corresponding author upon reasonable request.

Keywords

2D coordination networks, indigo, on-surface synthesis, scanning tunnelling microscopy, ultra-high vacuum

Received: May 15, 2025
Revised: October 8, 2025
Published online:

[1] C. A. Angell, *Science* **1995**, *267*, 1924.
[2] P. G. Debenedetti, F. H. Stillinger, *Nature* **2001**, *410*, 259.
[3] D. Shechtman, I. Blech, D. Gratias, J. W. Cahn, *Phys. Rev. Lett.* **1984**, *53*, 1951.
[4] E. E. Fry, J. Grimes, D. I. Stuart, *Mol. Biotechnol.* **1999**, *12*, 13.
[5] W. Steurer, S. Deloudi, *Acta Crystallogr., Sect. A:Found. Adv.* **2008**, *64*, 1.
[6] S. Boutet, L. Lomb, G. J. Williams, T. R. M. Barends, A. Aquila, R. B. Doak, U. Weierstall, D. P. DePonte, J. Steinbrener, R. L. Shoeman, M. Messerschmidt, A. Barty, T. A. White, S. Kassemeyer, R. A. Kirian, M. M. Seibert, P. A. Montanez, C. Kenney, R. Herbst, P. Hart, J. Pines, G. Haller, S. M. Gruner, H. T. Philipp, M. W. Tate, M. Hromalik, L. J. Koerner, N. van Bakel, J. Morse, W. Ghonsalves, et al., *Science* **2012**, *337*, 362.
[7] W. H. Zachariasen, *J. Am. Chem. Soc.* **1932**, *54*, 3841.
[8] T. A. Jung, R. R. Schlittler, J. K. Gimzewski, *Nature* **1997**, *386*, 696.
[9] J. V. Barth, G. Costantini, K. Kern, *Nature* **2005**, *437*, 671.
[10] L. Lichtenstein, M. Heyde, H. J. Freund, *J. Phys. Chem. C* **2012**, *116*, 20426.
[11] L. Lichtenstein, C. Buchner, B. Yang, S. Shaikhutdinov, M. Heyde, M. Sierka, R. Wlodarczyk, J. Sauer, H. J. Freund, *Angew. Chem., Int. Ed.* **2012**, *51*, 404.
[12] M. Heyde, S. Shaikhutdinov, H. J. Freund, *Chem. Phys. Lett.* **2012**, *550*, 1.
[13] J. F. Shackelford, B. D. Brown, *J. Non-Cryst. Solids* **1981**, *44*, 379.
[14] E. Limpert, W. A. Stahel, M. Abbt, *BioScience* **2001**, *51*, 341.
[15] N. Lin, S. Stepanow, M. Ruben, J. V. Barth, *Top. Curr. Chem.* **2009**, *287*, 1.
[16] J. V. Barth, *Surf. Sci.* **2009**, *603*, 1533.
[17] L. Dong, Z. A. Gao, N. Lin, *Prog. Surf. Sci.* **2016**, *91*, 101.
[18] R. Hou, C. Zhang, L. Xu, Y. Ding, W. Xu, *Phys. Chem. Chem. Phys.* **2025**, *27*, 8635.

[19] M. Marschall, J. Reichert, A. Weber-Bargioni, K. Seufert, W. Auwärter, S. Klyatskaya, G. Zoppellaro, M. Ruben, J. V. Barth, *Nat. Chem.* **2010**, *2*, 131.
[20] J. Reichert, M. Marschall, K. Seufert, D. Ecija, W. Auwärter, E. Arras, S. Klyatskaya, M. Ruben, J. V. Barth, *J. Phys. Chem. C* **2013**, *117*, 12858.
[21] D. Ecija, J. I. Urgel, A. C. Papageorgiou, S. Joshi, W. Auwarter, A. P. Seitsonen, S. Klyatskaya, M. Ruben, S. Fischer, S. Vijayaraghavan, J. Reichert, J. V. Barth, *Proc. Natl. Acad. Sci. U.S.A.* **2013**, *110*, 6678.
[22] J. I. Urgel, D. Écija, G. Q. Lyu, R. Zhang, C. A. Palma, W. Auwärter, N. A. Lin, J. V. Barth, *Nat. Chem.* **2016**, *8*, 657.
[23] X. Bouju, C. Mattioli, G. Franc, A. Pujol, A. Gourdon, *Chem. Rev.* **2017**, *117*, 1407.
[24] C.-A. Palma, J. Bjork, M. Bonini, M. S. Dyer, A. Llanes-Pallas, D. Bonifazi, M. Persson, P. Samorì, *J. Am. Chem. Soc.* **2009**, *131*, 13062.
[25] A. Llanes-Pallas, C.-A. Palma, L. Piot, A. Belbakra, A. Listorti, M. Prato, P. Samorì, N. Armaroli, D. Bonifazi, *J. Am. Chem. Soc.* **2009**, *131*, 509.
[26] A. Langner, S. L. Tait, N. Lin, C. Rajadurai, M. Ruben, K. Kern, *Proc. Natl. Acad. Sci. USA* **2007**, *104*, 17927.
[27] Z. L. Shi, N. Lin, *J. Am. Chem. Soc.* **2010**, *132*, 10756.
[28] G. Lyu, Q. Zhang, J. I. Urgel, G. Kuang, W. Auwärter, D. Écija, J. V. Barth, N. Lin, *Chem. Commun.* **2016**, *52*, 1618.
[29] J. Lu, D. Nieckarz, H. Jiang, Z. Zhu, Y. Yan, F. Zheng, W. Rżysko, J. Lisiecki, P. Szabelski, Q. Sun, *ACS Nano* **2023**, *17*, 20194.
[30] D. Ecija, S. Vijayaraghavan, W. Auwärter, S. Joshi, K. Seufert, C. Aurisicchio, D. Bonifazi, J. V. Barth, *ACS Nano* **2012**, *6*, 4258.
[31] H. Xu, R. Chakraborty, A. K. Adak, A. Das, B. Yang, D. Meier, A. Riss, J. Reichert, S. Narasimhan, J. V. Barth, A. C. Papageorgiou, *Angew. Chem., Int. Ed.* **2024**, *63*, 202319162.
[32] L. Meijer, N. Guyard, A.-L. Skaltsounis, G. Eisenbrand, Indirubin, the Red Shade of Indigo Life in Progress Edition, **2006**.
[33] D. V. Konarev, S. S. Khasanov, A. V. Kuzmin, A. F. Shestakov, A. Otsuka, H. Yamochi, G. Saito, R. N. Lyubovskaya, *Dalton Trans.* **2016**, *45*, 17095.
[34] F. S. Guo, R. A. Layfield, *Chem. Commun.* **2017**, *53*, 3130.
[35] D. V. Konarev, L. V. Zorina, S. S. Khasanov, A. F. Shestakov, A. M. Fatalov, A. Otsuka, H. Yamochi, H. Kitagawa, R. N. Lyubovskaya, *Inorg. Chem.* **2018**, *57*, 583.
[36] P. Mondal, A. Das, G. K. Lahiri, *Inorg. Chem.* **2016**, *55*, 1208.
[37] D. V. Konarev, S. S. Khasanov, A. F. Shestakov, A. M. Fatalov, M. S. Batov, A. Otsuka, H. Yamochi, H. Kitagawa, R. N. Lyubovskaya, *Dalton Trans.* **2017**, *46*, 14365.
[38] M. Chatterjee, P. Ghosh, K. Beyer, A. Paretzki, J. Fiedler, W. Kaim, G. K. Lahiri, *Chem. – Asian J.* **2018**, *13*, 118.
[39] W. Beck, K. Sunkel, *Z. Anorg. Allg. Chem.* **2020**, *646*, 248.
[40] E. Vorobyeva, F. Lissel, M. Salanne, M. R. Lukatskaya, *ACS Nano* **2021**, *15*, 15422.
[41] W. Kaim, G. K. Lahiri, *Coord. Chem. Rev.* **2019**, *393*, 1.
[42] E. D. Glowacki, G. Voss, N. S. Sariciftci, *Adv. Mater.* **2013**, *25*, 6783.
[43] Z. Shi, N. Lin, *J. Am. Chem. Soc.* **2009**, *131*, 5376.
[44] F. Bischoff, Y. He, K. Seufert, D. Stassen, D. Bonifazi, J. V. Barth, W. Auwärter, *Chem. – Eur. J.* **2016**, *22*, 15298.
[45] W. Xu, J.-g. Wang, M. Yu, E. Lægsgaard, I. Stensgaard, T. R. Linderoth, B. Hammer, C. Wang, F. Besenbacher, *J. Am. Chem. Soc.* **2010**, *132*, 15927.
[46] Y. Guo, A. Nuermaimaiti, N. D. Kjeldsen, K. V. Gothelf, T. R. Linderoth, *J. Am. Chem. Soc.* **2020**, *142*, 19814.
[47] P. Y. Huang, S. Kurasch, A. Srivastava, V. Skakalova, J. Kotakoski, A. V. Krasheninnikov, R. Hovden, Q. Y. Mao, J. C. Meyer, J. Smet, D. A. Muller, U. Kaiser, *Nano Lett.* **2012**, *12*, 1081.
[48] N. Ma, S. Horike, *Chem. Rev.* **2022**, *122*, 4163.
[49] G. Di Santo, C. Castellarin-Cudia, M. Fanetti, B. Taleatu, P. Borghetti, L. Sangaletti, L. Floreano, E. Magnano, F. Bondino, A. Goldoni, *J. Phys. Chem. C* **2011**, *115*, 4155.
[50] C. Shen, M. Haryono, A. Grohmann, M. Buck, T. Weidner, N. Ballav, M. Zharnikov, *Langmuir* **2008**, *24*, 12883.
[51] Y. Zubavichus, M. Zharnikov, Y. J. Yang, O. Fuchs, E. Umbach, C. Heske, A. Ulman, M. Grunze, *Langmuir* **2004**, *20*, 11022.
[52] S. L. Tait, Y. Wang, G. Costantini, N. Lin, A. Baraldi, F. Esch, L. Petaccia, S. Lizzit, K. Kern, *J. Am. Chem. Soc.* **2008**, *130*, 2108.
[53] H. Shan, L. W. Zhou, W. Ji, A. D. Zhao, *J. Phys. Chem. Lett.* **2021**, *12*, 10808.
[54] J. Rodriguez-Fernandez, Z. Z. Sun, L. Zhang, T. Tan, A. Curto, J. Fester, A. Vojvodic, J. V. Lauritsen, *J. Chem. Phys.* **2019**, 150.
[55] M. Q. Hua, B. W. Xia, M. Wang, E. Li, J. Liu, T. H. Wu, Y. F. Wang, R. N. Li, H. H. Ding, J. Hu, Y. F. Wang, J. F. Zhu, H. Xu, W. Zhao, N. Lin, *J. Phys. Chem. Lett.* **2021**, *12*, 3733.
[56] P. Knecht, N. Suryadevara, B. D. Zhang, J. Reichert, M. Ruben, J. V. Barth, S. Klyatskaya, A. C. Papageorgiou, *Chem. Commun.* **2018**, *54*, 10072.
[57] Z. L. Shi, J. Liu, T. Lin, F. Xia, P. N. Liu, N. Lin, *J. Am. Chem. Soc.* **2011**, *133*, 6150.
[58] P. Zalake, S. Ghosh, S. Narasimhan, K. G. Thomas, *Chem. Mater.* **2017**, *29*, 7170.
[59] B. E. Warren, J. Biscce, *J. Am. Ceram. Soc.* **1938**, *21*, 49.
[60] J. F. Shackelford, *J. Non-Cryst. Solids* **1982**, *49*, 299.
[61] C. Buechner, L. W. Liu, S. Stuckenholz, K. M. Burson, L. Lichtenstein, M. Heyde, H. J. Gao, H. J. Freund, *J. Non-Cryst. Solids* **2016**, *435*, 40.
[62] L. Lichtenstein, M. Heyde, H. J. Freund, *Phys. Rev. Lett.* **2012**, *109*.
[63] I. Horcas, R. Fernández, J. M. Gómez-Rodríguez, J. Colchero, J. Gómez-Herrero, A. M. Baro, *Rev. Sci. Instrum.* **2007**, *78*, 013705.
[64] A. Riss, *J. Open Source Softw.* **2022**, *7*, 4644.
[65] P. Giannozzi, S. Baroni, N. Bonini, M. Calandra, R. Car, C. Cavazzoni, D. Ceresoli, G. L. Chiarotti, M. Cococcioni, I. Dabo, A. Dal Corso, S. de Gironcoli, S. Fabris, G. Fratesi, R. Gebauer, U. Gerstmann, C. Gougoussis, A. Kokalj, M. Lazzeri, L. Martin-Samos, N. Marzari, F. Mauri, R. Mazzarello, S. Paolini, A. Pasquarello, L. Paulatto, C. Sbraccia, S. Scandolo, G. Sclauzero, A. P. Seitsonen, et al., *J. Phys.: Condens. Matter* **2009**, *21*.
[66] P. E. Blöchl, O. Jepsen, O. K. Andersen, *Phys. Rev. B* **1994**, *49*, 16223.
[67] I. Hamada, *Phys. Rev. B* **2014**, *89*, 121103.
[68] K. Lee, É. D. Murray, L. Kong, B. I. Lundqvist, D. C. Langreth, *Phys. Rev. B* **2010**, *82*, 081101.
[69] M. Cococcioni, S. de Gironcoli, *Phys. Rev. B* **2005**, *71*, 035105.
[70] C. G. Broyden, J. E. Dennis, J. J. Moré, *IMA J. Appl. Math.* **1973**, *12*, 223.
[71] R. Fletcher, *Comput. J.* **1970**, *13*, 317.
[72] D. Goldfarb, *Math. Comput.* **1970**, *24*, 23.
[73] D. F. Shanno, *Math. Comput.* **1970**, *24*, 647.
[74] N. Marzari, D. Vanderbilt, A. De Vita, M. C. Payne, *Phys. Rev. Lett.* **1999**, *82*, 3296.
[75] J. Tersoff, D. R. Hamann, *Phys. Rev. B* **1985**, *31*, 805.